

## Article

# Immobilization of Rh(I)-N-Xantphos and Fe(II)-C-Scorpionate onto Magnetic Nanoparticles: Reusable Catalytic System for Sequential Hydroformylation/Acetalization

Fábio M. S. Rodrigues <sup>1</sup>, Lucas D. Dias <sup>1,2</sup>, Mário J. F. Calvete <sup>1</sup>, Teresa M. R. Maria <sup>1</sup>, Liane M. Rossi <sup>3</sup>, Armando J. L. Pombeiro <sup>4</sup>, Luísa M. D. R. S. Martins <sup>4</sup> and Mariette M. Pereira <sup>1,\*</sup>

<sup>1</sup> Centro de Química de Coimbra, Departamento de Química Rua Larga, Universidade de Coimbra, 3004-535 Coimbra, Portugal; fms\_rodrigues@hotmail.com (F.M.S.R.); lucasdanillodias@gmail.com (L.D.D.); mcalvete@qui.uc.pt (M.J.F.C.); troseiro@ci.uc.pt (T.M.R.M.)

<sup>2</sup> São Carlos Institute of Physics, University of São Paulo, São Carlos-SP 13566-590, Brazil

<sup>3</sup> Departamento de Química Fundamental, Instituto de Química, Universidade de São Paulo, São Paulo-SP 05508-000, Brazil; lrossi@iq.usp.br

<sup>4</sup> Centro de Química Estrutural, Instituto Superior Técnico, Universidade de Lisboa, Av. Rovisco Pais, 1049-001 Lisboa, Portugal; pombeiro@ist.utl.pt (A.J.L.P.); luisamargaridamartins@tecnico.ulisboa.pt (L.M.D.R.S.M.)

\* Correspondence: mmpereira@qui.uc.pt



**Citation:** Rodrigues, F.M.S.; Dias, L.D.; Calvete, M.J.F.; Maria, T.M.R.; Rossi, L.M.; Pombeiro, A.J.L.; Martins, L.M.D.R.S.; Pereira, M.M. Immobilization of Rh(I)-N-Xantphos and Fe(II)-C-Scorpionate onto Magnetic Nanoparticles: Reusable Catalytic System for Sequential Hydroformylation/Acetalization. *Catalysts* **2021**, *11*, 608. <https://doi.org/10.3390/catal11050608>

Academic Editor: Alain Roucoux

Received: 18 April 2021

Accepted: 4 May 2021

Published: 10 May 2021

**Publisher's Note:** MDPI stays neutral with regard to jurisdictional claims in published maps and institutional affiliations.



**Copyright:** © 2021 by the authors. Licensee MDPI, Basel, Switzerland. This article is an open access article distributed under the terms and conditions of the Creative Commons Attribution (CC BY) license (<https://creativecommons.org/licenses/by/4.0/>).

**Abstract:** Two heterogeneous catalysts, MNP@SiO<sub>2</sub>-N-Xantphos/Rh(I) and MNP@SiO<sub>2</sub>-NH-C-scorpionate/Fe(II), were prepared by reaction of chloro-functionalized MNP@SiO<sub>2</sub> with N-Xantphos and amino-functionalized MNP@SiO<sub>2</sub> with iron(II)/C-allyl-scorpionate through nucleophilic substitution and hydroaminomethylation reactions, respectively. All catalysts were characterized using standard spectroscopic means, transmission electron microscopy (TEM), thermogravimetry (TG), and inductively coupled plasma optical emission spectrometry (ICP-OES). An active and highly selective one-pot hydroformylation/acetalization homogeneous system for the transformation of terminal and highly substituted olefins (including terpenes) onto ethyl acetals is described. A synergic effect of bimetallic Rh(I)/P and Fe(II)/C-scorpionate catalysts is disclosed for the first time. The further sequential use of the heterogeneous catalysts, MNP@SiO<sub>2</sub>-N-Xantphos/Rh(I) and MNP@SiO<sub>2</sub>-NH-C-scorpionate/Fe(II) in hydroformylation/acetalization reactions allows the direct transformation of olefin onto ethyl acetals, keeping the activity and selectivity. Both catalysts were easily recovered by magnetic separation and reused with negligible loss of activity/selectivity, after six reutilization cycles.

**Keywords:** hydroformylation; acetalization; heterogeneous catalysis; sequential process; terpenes

## 1. Introduction

Nowadays, one of the ultimate goals for synthetic chemists is to mimic natural systems for the construction of complex molecules using sequential catalysis [1–3]. Catalytic hydroformylation has been used as a central reaction in several sequential processes to produce high-value products directly from olefins, such as alcohols, acetals, amines, and others [4–11]. We highlight the hydroformylation/acetalization reaction that allows the direct transformation of olefins into high-value oxygenated products in a sequential process without isolation of the aldehyde intermediates [12–17], including in the valorization of terpenes [18,19]. Nevertheless, these processes still have issues associated with the catalyst reutilization. Therefore, advances in selective catalytic processes, using homogeneous catalysts immobilized onto solid supports, are amongst the main challenges for the translation of academically developed catalysts towards sustainable industrial processes [20]. Homogeneous hydroformylation is one of the highly significant catalyzed industrial process for the production of aldehydes from olefins through addition of syngas (CO/H<sub>2</sub>),

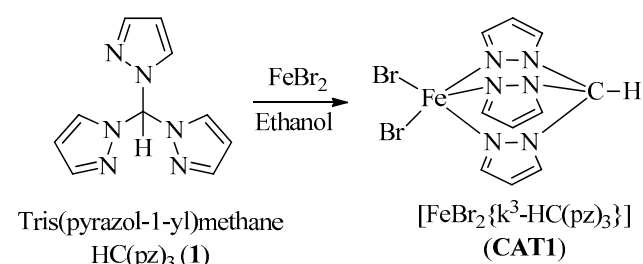
usually promoted by rhodium/P-ligands-based catalysts [5,21]. However, high rhodium prices lead to the quest for efficient and reusable alternative catalytic systems based on the development of immobilized rhodium type catalysts. These heterogeneous catalysts can be prepared using several methodologies including covalent linkage using functionalized ligands; dispersion of solid nanoparticles in solid materials; metal single atoms deposited in solid supports and metal ionic complexes can be immobilized into a supported ionic liquid phase (SILP) [22–26]. Particularly, the immobilization of Rh(I)/Xantphos derivatives demonstrate the interest in developing highly selective heterogeneous catalysts to produce terminal oxo products [27–29], with specific interest on the use of magnetic nanoparticles (MNP) as supports, since they allow catalyst reutilization by simple use of external magnets [30,31]. Furthermore, a few examples of heterogeneous catalysts for the sequential hydroformylation/acid catalyzed acetalization of olefins, mostly using ionic liquids as solvents [12,32–34], and biphasic systems using sulfonated phosphines [35,36] have been reported. So far, to the best of our knowledge, C-scorpionate metal complexes, including iron-based complexes, have been largely applied as catalysts for several reactions [37–40], and extended to utilization of immobilized C-scorpionate complexes [41–45]. However, covalent immobilization of such complexes was never reported, particularly, the use of a Rh–P/Fe–C-scorpionate bimetallic catalytic system for implementation of sequential hydroformylation/acetalization transformations.

Herein, we describe the immobilization of Fe(II)/C-scorpionate and N-Xantphos onto 3-aminopropyl-functionalized iron magnetic nanoparticles (MNP@SiO<sub>2</sub>-NH<sub>2</sub>), through hydroaminomethylation [46], and nucleophilic substitution reactions, respectively. Then, the bimetallic catalytic system, Rh(I)/Xantphos and Fe(II)-C-scorpionate [FeBr<sub>2</sub>{κ<sup>3</sup>-HC(pz)<sub>3</sub>}] (pz = pyrazolyl), was evaluated in sequential hydroformylation/acetalization of olefins under homogeneous and heterogeneous conditions. Reutilization studies of the catalysts are also described.

## 2. Results and Discussion

### 2.1. Synthesis and Characterization of Catalysts

The iron(II)-C-scorpionate catalyst (**CAT1**) was synthesized by slight modifications of previously described methods [47,48] (Scheme 1). An ethanol solution of Ligand HC(pz)<sub>3</sub> (**1**) was added dropwise to a room temperature stirred iron(II) bromide ethanol solution, under inert atmosphere providing, after 2 h, [FeBr<sub>2</sub>{κ<sup>3</sup>-HC(pz)<sub>3</sub>}] (**CAT1**) in 91% yield. Samples of **CAT1** were characterized by <sup>1</sup>H- and <sup>13</sup>C-NMR spectroscopy, HRMS, and IR spectroscopy (see SI).



**Scheme 1.** Synthesis of **CAT1**.

Catalysts **CAT2**, **CAT3**, and **CAT4** were prepared in situ, using the known P-ligands and corresponding rhodium salts. (Figure 1, **L1** = Xantphos, **L2** = triphenylphosphine, or **L3** = *tris*[(R)-2'-(benzyloxy)-1,1'-binaphthyl-2-yl] phosphite [49]) with the commercially available pre-catalyst [Rh(acac)(CO)<sub>2</sub>] (see experimental section).

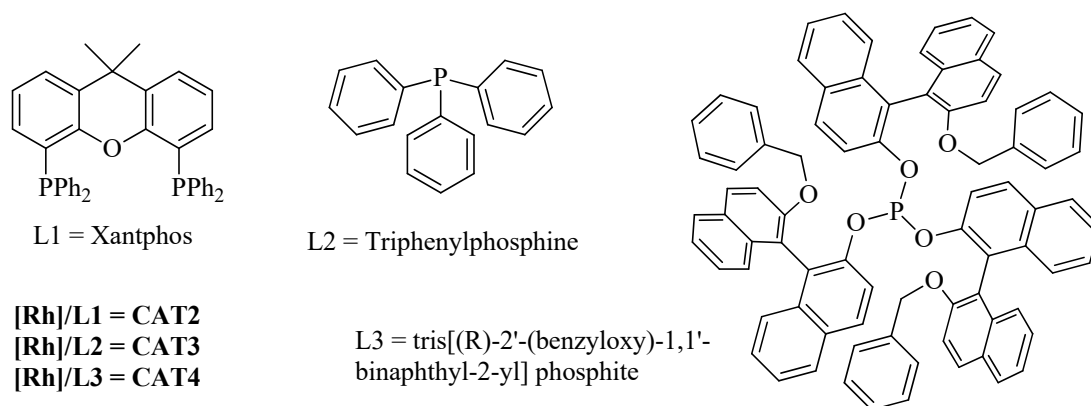


Figure 1. P-ligands used in the homogeneous studies.

Heterogeneous catalysts (CAT5 and CAT6, Figure 2) were prepared through the synthesis and 3-aminopropyl functionalization of core-shell magnetic iron nanoparticles, followed by covalent grafting of the suitable functionalized homogeneous ligand.

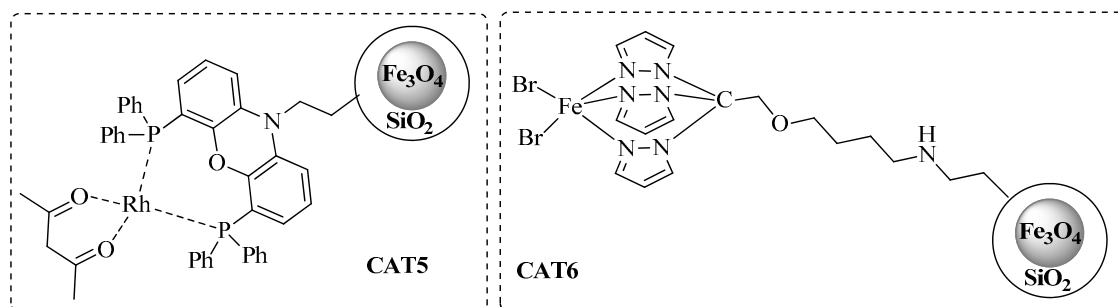
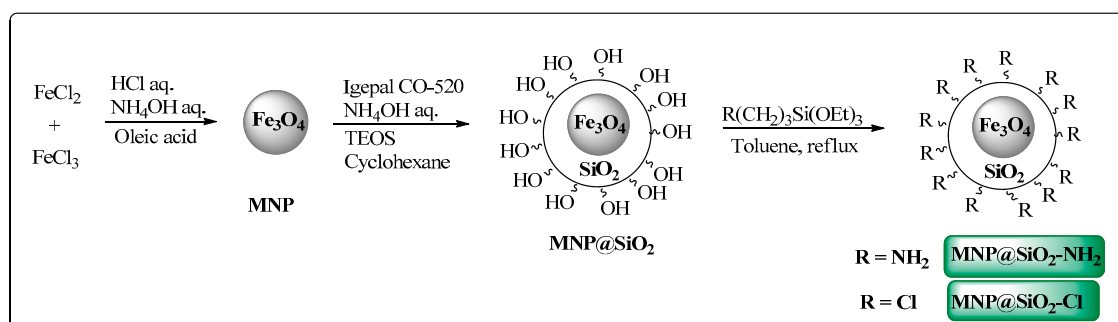


Figure 2. Heterogeneous catalysts for hydroformylation/acetalization of olefins.

The magnetic nanoparticles were obtained through preparation of magnetite (MNP) followed by silica coating with further 3-amino- or 3-chloropropyl-functionalization (Scheme 2).



Scheme 2. Synthetic route for functionalized iron core-shell magnetic nanoparticles (MNP@SiO<sub>2</sub>-Cl and MNP@SiO<sub>2</sub>-NH<sub>2</sub>).

The MNP were prepared by co-precipitation method using Fe<sup>2+</sup>/Fe<sup>3+</sup> ions under alkaline reaction conditions, followed by stabilization with oleic acid addition at 10,000 rpm [50]. Transmission electronic microscopy (TEM) analysis of MNP shows the formation of magnetite nanoparticles (≈7 nm) (Figure S5). Then, MNP@SiO<sub>2</sub> were prepared according to a previously described method [51], by reacting MNP with tetraethyl orthosilicate (TEOS) under alkaline conditions. MNP@SiO<sub>2</sub> were obtained with approximately 23 nm size, as shown in the TEM analysis, (Figure S6). All particle size measurements were performed in triplicate. Additionally, the obtained material was analyzed by thermogravimetry (TG). The MNP@SiO<sub>2</sub> thermogram (Figure 3a) shows a weight loss in the temperature range of

50–150 °C, attributed to the loss of adsorbed water and solvents. Another 1.5% weight loss occurred between 200 and 800 °C, which can be attributed to the decomposition of silanol groups of MNP@SiO<sub>2</sub>.

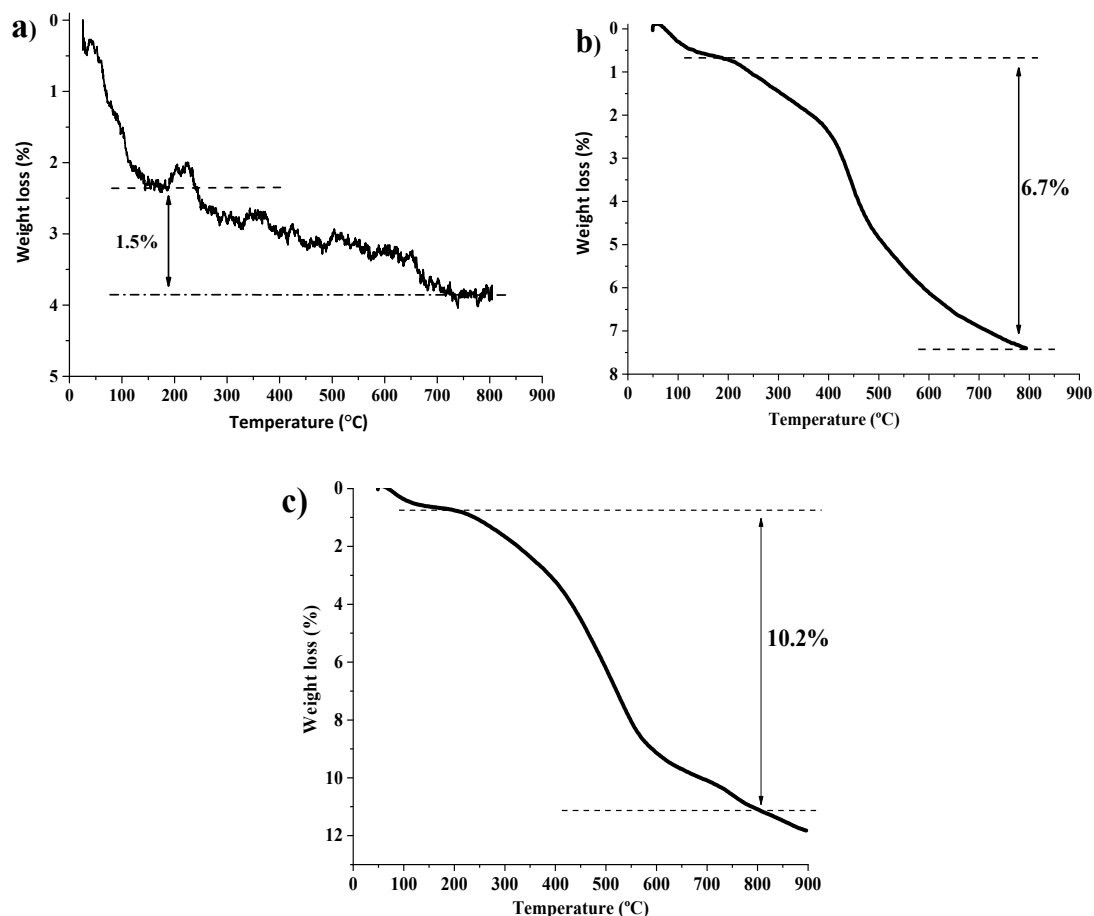
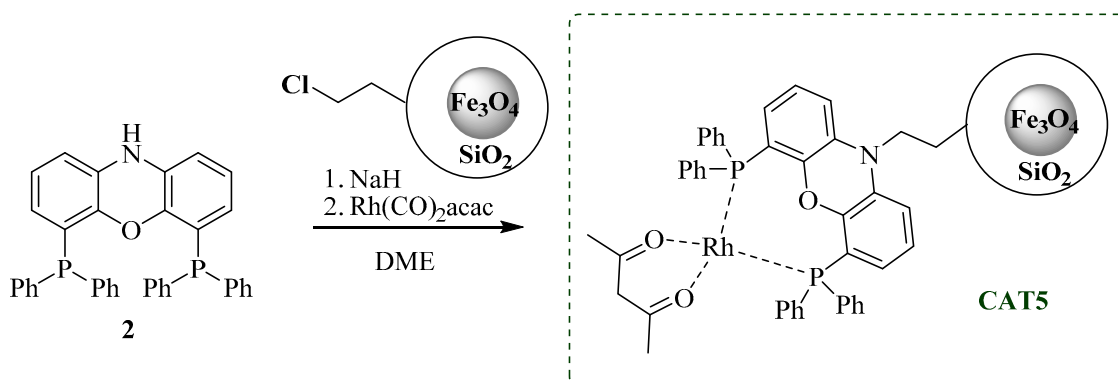


**Figure 3.** (a) TG curve of MNP@SiO<sub>2</sub>, (b) TG curve of MNP@SiO<sub>2</sub>-Cl, and (c) TG curve of MNP@SiO<sub>2</sub>-NH<sub>2</sub>.

Then, the 3-chloropropyl-functionalized MNPs were prepared by nucleophilic substitution reaction of MNP@SiO<sub>2</sub> with (3-chloropropyl)triethoxysilane (CPTES). The resulting material MNP@SiO<sub>2</sub>-Cl was magnetically collected, washed and dried and characterized by TG analysis, (Figure 3b). The thermogram of MNP@SiO<sub>2</sub>-Cl shows a weight loss of 6.7% between 200 and 800 °C, which represents a 5.2% weight loss, attributed to the loss of 3-chloropropyl groups, considering that a 1.5% weight loss is ascribed to decomposition of silanol groups. This weight-loss corresponds to 0.66 mmol of 3-chloropropyl groups/g of MNP@SiO<sub>2</sub>-Cl material. Moreover, the amino-functionalized MNPs were prepared by reaction of MNP@SiO<sub>2</sub> with 3-aminopropyltriethoxysilane (APTES), using a similar approach. The resulting MNP@SiO<sub>2</sub>-NH<sub>2</sub> material was then characterized by comparison of Fourier-transform infrared spectroscopy (FTIR) spectrum with the initial MNP@SiO<sub>2</sub> spectrum (Figure S7), which confirmed the desired 3-aminopropyl-functionalization [52]. Additionally, MNP@SiO<sub>2</sub>-NH<sub>2</sub> was also characterized by TG, Figure 3c. A weight loss between 50 and 200 °C, attributed to loss of adsorbed water and vestigial organic solvents, was observed. Another weight loss (10.2%), in the temperature range 200–800 °C, was attributed to the decomposition of silanol and 3-aminopropyl groups. Subtracting the contribution of the silanol groups decomposition (1.5%), we obtain 8.7% wt loss, attributed to the aminopropyl groups, which indicates that the material has 1.48 mmol of propylamine groups/g of MNP@SiO<sub>2</sub>-NH<sub>2</sub> material.

Aiming to promote the covalent immobilization of the homogeneous rhodium catalytic system, *N*-Xantphos (**2**) was selected as a functionalized analog of the Xantphos ligand, used as model in the homogeneous catalytic studies. Therefore, we performed a nucleophilic substitution reaction between *N*-Xantphos and MNP@SiO<sub>2</sub>-Cl, using NaH as base and dry DME as solvent, under inert atmosphere for 15 h. Upon workup, [Rh(acac)(CO)<sub>2</sub>] and freshly dried DME were added, and the mixture was stirred for another 6 h, after which the collected and purified catalyst was dried under vacuum and stored (Scheme 3).



**Scheme 3.** Preparation of Rh-immobilized catalyst **CAT5**.

The resulting material (**CAT5**) was analyzed by TG and inductively coupled plasma optical emission spectrometry (ICP-OES) analysis. The thermogram of **CAT5** (Figure 4a) presents a weight loss of 13.5% between 200 and 800 °C, which is attributed to degradation of total organic material present in the nanoparticles. The amount of immobilized *N*-Xantphos type ligand was calculated by the difference between the total amount of organic residue (13.5%) and the organic contribution of MNP@SiO<sub>2</sub>-Cl (6.7% weight loss). Therefore, the 6.8% weight loss is attributed to *N*-Xantphos ligand, corresponding to approximately 0.12 mmol of organic material per each gram of solid material. Additionally, ICP-OES analysis corroborated the presence of Rh, 0.061 mmol per gram of solid material, suggesting that 50% of the immobilized *N*-Xantphos ligand is complexed with Rh metal. In order to promote the covalent immobilization of the Fe(II)C-scorpionate type ligands onto aminated nanoparticles (MNP@SiO<sub>2</sub>-NH<sub>2</sub>), we hypothesized to use a hydroaminomethylation reaction approach (Scheme 4).

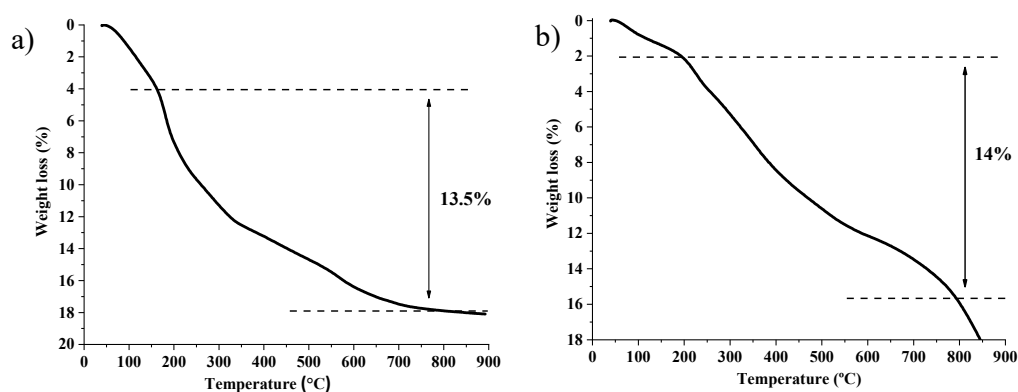
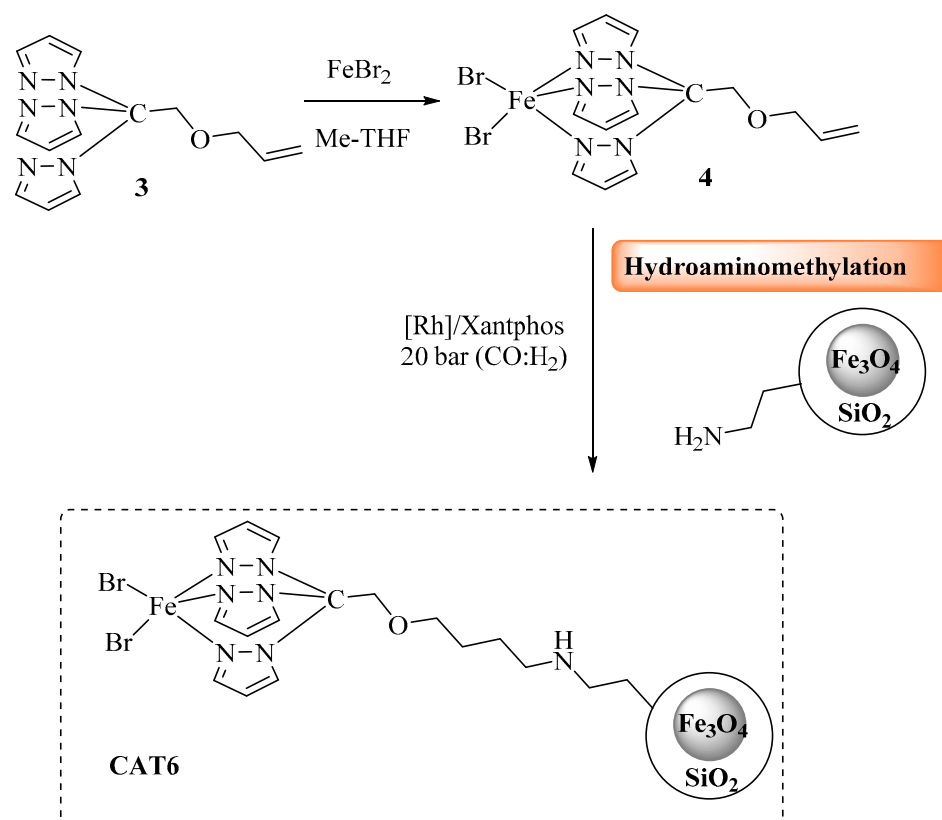


**Figure 4.** (a) TG curve of **CAT5** and (b) TG curve of **CAT6**.



**Scheme 4.** Preparation of  $[\text{FeBr}_2\{\text{HC}(\text{pz})_3\}]$  immobilized catalyst **CAT6** via hydroaminomethylation reaction.

An allyl group was covalently linked to  $\text{HC}(\text{pz})_3$  ligand [53], followed by complexation with  $\text{FeBr}_2$  [47], using green-source solvent 2-MeTHF [54], to provide **3**. Then, complexation with iron(II) bromide afforded the new complex  $[\text{FeBr}_2\{\text{allyl-HC}(\text{pz})_3\}]$  (**4**) in 95% yield. Finally, compound **4**,  $[\text{Rh}(\text{acac})(\text{CO})_2]/\text{Xantphos}$ , the aminated magnetic  $\text{MNP@SiO}_2\text{-NH}_2$  (1.48 mmol  $\text{NH}_2/\text{g}$  material), and anisole as solvent were reacted under hydroaminomethylation conditions (first 30 bar with 1:1  $\text{CO}/\text{H}_2$ , for 48 h and then 30 bar with  $\text{H}_2$ , for 4 h), at 65 °C. The desired **CAT6** material was then isolated from the reaction medium by simple application of an external magnet. The resulting material was analyzed through ICP-OES analysis, and **CAT6** did not show presence of Rh. TG analysis of **CAT6** (Figure 4b) revealed a weight loss of 14% in the range of 200–800 °C, which is attributed to degradation of total organic material.

The amount of immobilized C-scorpionate type ligand was calculated by the difference between the total amount of organic residue (14%) and the organic part of  $\text{MNP@SiO}_2\text{-NH}_2$  (10.2% weight loss). Therefore, 3.8% weight loss was attributed to the C-scorpionate organic residue, which corresponds to approximately 0.13 mmol of immobilized C-scorpionate type ligand per gram of material. Since **CAT6** contains iron in the nanoparticles core, the amount of immobilized iron complex was calculated through the difference between the molar amount of **4** added to the immobilization reaction (2 mmol) and the value of the iron recovered from the **CAT6** isolation washing process obtained by ICP-OES analysis (1.89 mmol). The obtained value was 0.12 mmol of iron complex per gram of material, and this was the value used for the calculations in heterogeneous catalytic reactions. Furthermore, the ICP analysis of **CAT6** did not show the presence of Rh.

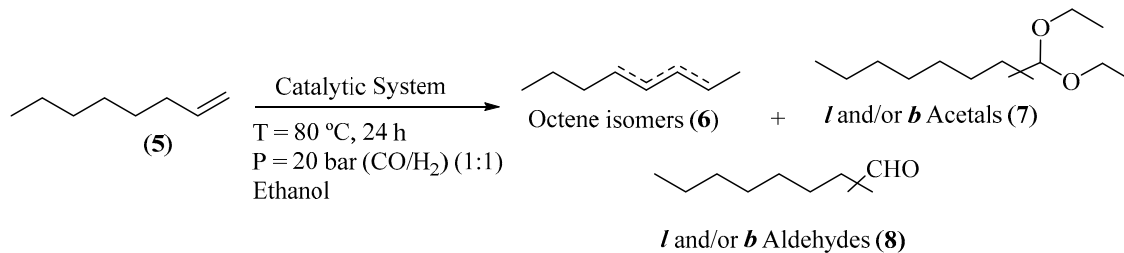
## 2.2. Homogeneous Hydroformylation/Acetalization of Olefins

Before the implementation of the heterogeneous sequential bimetallic catalytic system, we started by the optimization of the homogeneous sequential catalytic system, using oct-

1-ene as model substrate and ethanol as nucleophile, under 20 bar (CO/H<sub>2</sub>, 1:1) constant pressure and temperature of 80 °C (Table 1). First, we evaluated the use of [Rh(acac)(CO)<sub>2</sub>] as catalyst in the sequential hydroformylation/acetalization of oct-1-ene, and a near-complete olefin conversion (93%) was observed by GC analysis, after 24 h. Nevertheless, very low chemoselectivity for aldehydes (19%) and acetals (21%) was achieved, being internal isomers (60%) the main products (Table 1, Entry 1). Then, we evaluated the effect of the addition of ligand HC(pz)<sub>3</sub> (**1**) to the system containing [Rh(acac)(CO)<sub>2</sub>] (Rh/(**1**) = 1:2.5) and again 95% conversion was obtained, but in this case with similar chemoselectivity for aldehydes (20%) and higher for acetals (34%), besides a lower amount of internal alkene isomers (46%) (Table 1, Entry 2). Additionally, the use of the bimetallic combination based on [Rh(acac)(CO)<sub>2</sub>] with [FeBr<sub>2</sub>{κ<sup>3</sup>-HC(pz)<sub>3</sub>}] (**CAT1**) provided full conversion of oct-1-ene, with high selectivity for oxo products, including 47% acetal chemoselectivity, with concomitant low isomerization (36%). These results evidence the beneficial effect of [FeBr<sub>2</sub>{κ<sup>3</sup>-HC(pz)<sub>3</sub>}] (**CAT1**) as a promising sustainable catalyst to enable the direct one-pot transformation of olefins toward acetals (Table 1, Entry 3). Next, to avoid initial isomerization and enhance the rate of aldehyde formation, we evaluated the use of the same Rh(I)/Fe(II) bimetallic system, but using a Rh/P-ligand modified catalyst (P = Xantphos, PPh<sub>3</sub>, or the bulky *tris*[(*R*)-2'-(benzyloxy)-1,1'-binaphthyl-2-yl] phosphite; Figure 1). The results are presented in Table 1 (Entries 4–6). These results suggest that the combination of [Rh(acac)(CO)<sub>2</sub>]/Xantphos (**CAT2**) with the C-scorpionate [FeBr<sub>2</sub>{κ<sup>3</sup>-HC(pz)<sub>3</sub>}] (**CAT1**) produced the most active (99% conversion) and selective system, with 82% chemoselectivity for acetals and 93% regioselectivity for the linear isomer, as expected for high bite angle phosphines like Xantphos (111°) [55,56], (Table 1, Entry 4). Additionally, the catalytic system using triphenylphosphine as Rh-P-ligand system (**CAT3**), gave 97% conversion and 87% acetal chemoselectivity, but with only 66% of regioselectivity for linear acetal (Table 1, Entry 5). Moreover, the combination of [Rh(acac)(CO)<sub>2</sub>]/bulky phosphite (**CAT4**) with [FeBr<sub>2</sub>{κ<sup>3</sup>-HC(pz)<sub>3</sub>}] (**CAT1**) led to an active hydroformylation/acetalization system (99% conversion), with high chemoselectivity for acetals (91%), but, as expected, with lower regioselectivity for the linear isomer (69%) (Table 1, Entry 6). This outcome may be attributed to the concomitant hydroformylation of internal double bonds, typical of Rh/bulky phosphite systems [57–61].

These results corroborate the versatility of these Rh(I)/P-ligand, Fe(II)/C-scorpionate bimetallic systems to promote the direct transformation of olefins into value-added acetals, with chemo and regioselectivity modulated by the P-ligands, always with high oxo-product selectivity. Additionally, we evaluated the activity of the Fe(II)/C-scorpionate catalyst (**CAT1**) in the hydroformylation reaction of oct-1-ene and in the direct acetalization of nonanal (Table 1, Entries 7–8). Regarding the exclusive use of **CAT1** in the hydroformylation reaction, no conversion was observed (Table 1, Entry 7). Conversely, **CAT1** demonstrated to be an active Lewis acid catalyst to promote the acetalization of nonanal (95% acetal; Table 1, Entry 8). The reaction progress for the sequential hydroformylation/acetalization process, using the bimetallic **CAT2**/**CAT1** system, is illustrated in Figure 5.

From the analysis of Figure 5, nearly 75% olefin conversion was achieved after just 1 h (51% selectivity for aldehydes and 20% for acetals). As expected, after this period, the yield of aldehydes started to decrease with concomitant increase in acetal formation throughout the experiment. The kinetic profile of the bimetallic catalytic system shows that both the hydroformylation (*k*<sub>1</sub>) and acetalization (*k*<sub>2</sub>) rates decrease over time, suggesting that the hydroformylation rate is dependent on olefin concentration and the acetal formation is dependent on aldehyde concentration. After 24 h, 99% of oct-1-ene conversion was observed, with 79% acetals, and 16% of non-converted aldehydes, besides 4% of oct-1-ene isomers which was constant during the experiment (Figure 5). Scheme 5 illustrates the simplified mechanism pathways for the direct synthesis of acetals from terminal alkyl olefins [62,63]. As known, the Rh(I)/Xantphos catalyst (**CAT2**) catalyzes the regioselective formation of linear aldehyde. Then, the presence of **CAT1** (Fe(II)/C-scorpionate), an appropriate Lewis acid, and ethanol promotes the sequential transformation of the aldehyde into ethyl acetal.

**Table 1.** Sequential hydroformylation/acetalization of oct-1-ene: optimization studies <sup>[a]</sup>.

Entry.	Catalytic System	Conversion (%) <sup>[b]</sup>	Selectivity (%) <sup>[b]</sup> ( <i>l</i> : <i>b</i> )		
			6	7	8
1	[Rh(acac)(CO) <sub>2</sub> ]	93	60	21 (38:62)	19 (23:77)
2	[Rh(acac)(CO) <sub>2</sub> ] HC(pz) <sub>3</sub> (1)	95	46	34 (44:56)	20 (18:82)
3	[Rh(acac)(CO) <sub>2</sub> ] CAT1	99	36	47 (61:39)	17 (27:73)
4	CAT2 CAT1	99	3	82 (93:7)	15 (80:20)
5	CAT3 CAT1	97	1	87 (66:34)	12 (24:76)
6	CAT4 CAT1	99	-	91 (69:31)	9 (32:68)
7	CAT1	1	-	-	-
8 <sup>[c]</sup>	CAT1	95	-	100	-

<sup>[a]</sup> Reaction conditions: oct-1-ene 3.00 mmol, [Rh(acac)(CO)<sub>2</sub>] 0.02 mmol, P-ligand (CAT2: 0.05 mmol, CAT3: 0.10 mmol, CAT4: 0.10 mmol), CAT1 (0.05 mmol) or (1) 0.05 mmol, ethanol (6 mL), 20 bar CO/H<sub>2</sub> (1:1) at 80 °C for 24 h. <sup>[b]</sup> Determined by GC-MS analysis using isooctane as an external standard. <sup>[c]</sup> Nonanal (3 mmol) was used as substrate.

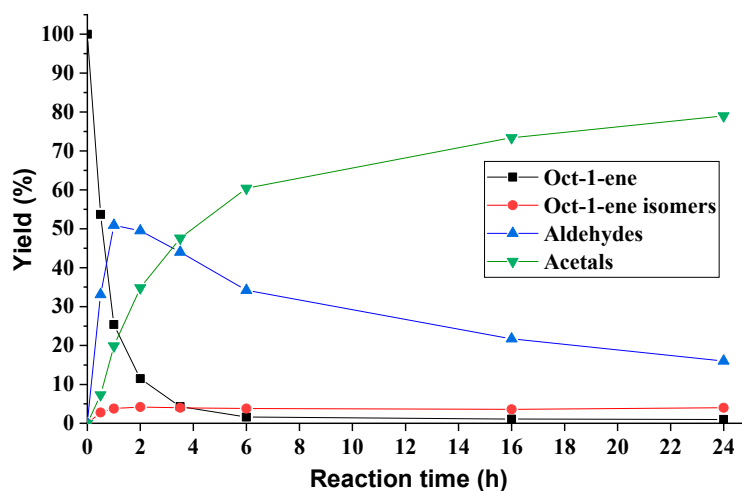
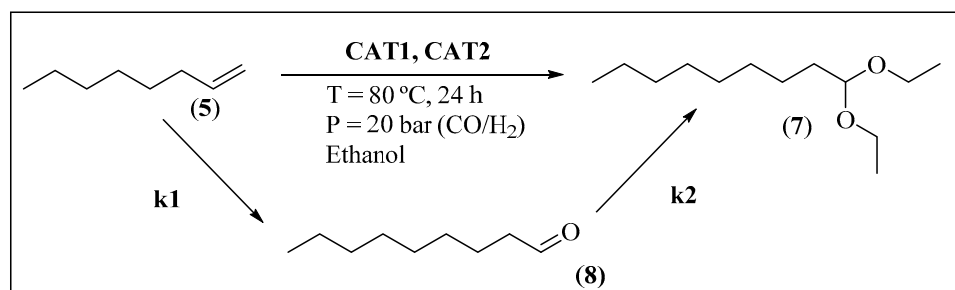
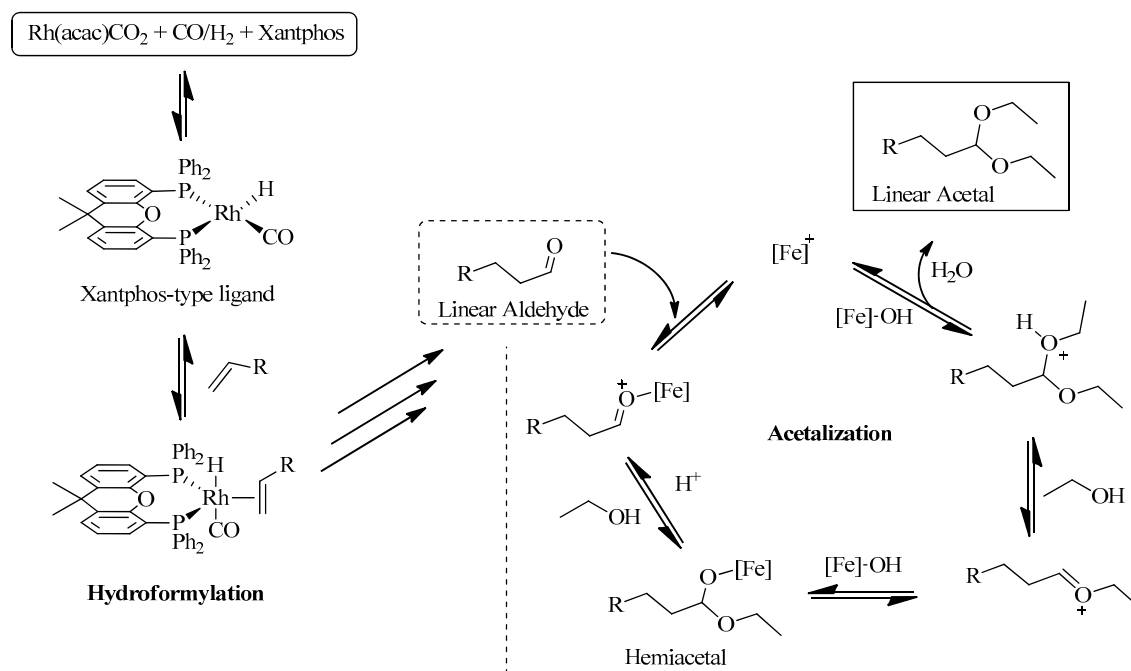


**Figure 5.** Reaction progress of hydroformylation/acetalization of oct-1-ene: Substrate and product yield vs. reaction time. Reaction conditions: olefin 6.00 mmol, CAT2 0.04 mmol, CAT1 0.10 mmol, ethanol 12 mL; P = 20 bar (CO/H<sub>2</sub>); and T = 80 °C. Yield determined by GC analysis of aliquots from the crude reaction using isooctane as an external standard.



**Scheme 5.** Proposed simplified mechanisms for hydroformylation/acetalization of olefins with **CAT2** ( $[\text{Rh}(\text{acac})(\text{CO})_2]/\text{Xantphos}$ ) and **CAT1** ( $[\text{FeBr}_2\{\kappa^3\text{HC}(\text{pz})_3\}]$ ), here represented by  $[\text{Fe}]$ .

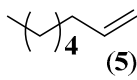
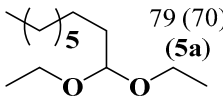
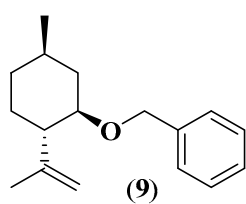
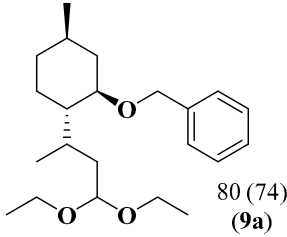
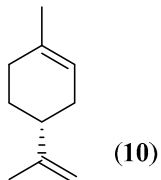
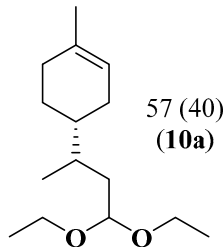
In order to study the synergic effect of the combination of P-ligand based hydroformylation catalysts (**CAT2** or **CAT4**) with iron(II)-C-scorpionate-based acetalization catalyst (**CAT1**) in the sequential hydroformylation/acetalization process, we pursued these studies with the use of Rh(I)/ tris[(R)-2'-(benzyloxy)-1,1'-binaphthyl-2-yl] phosphite (**CAT4**) in the hydroformylation reaction, since it is a known active catalyst for hydroformylation of highly substituted olefins [60–65]. Thus, the replacement of Rh(I)/Xantphos (**CAT2**) (Table 2, Entry 1) by the bulky Rh/tris[(R)-2'-(benzyloxy)-1,1'-binaphthyl-2-yl] phosphite (**CAT4**) allowed the direct transformation of di and tri-substituted olefins of terpenes ((-)-isopulegol benzyl ether derivative **7** and (+)-limonene **8**) into the corresponding acetals in 80% and 90% yields, respectively (Table 2, Entries 2,3). It should be mentioned that this is the first catalytic system that allows the formation of acetals derived from both, di and trisubstituted limonene double bonds using mild reaction conditions. This result discloses the high activity of **CAT4** to promote the hydroformylation of highly substituted olefins when compared with Gusevskaya work [19], where only the terminal exocyclic  $\beta$ -citronellene double bond was converted to acetal, even using harsher reaction conditions (80 bar of  $\text{CO}/\text{H}_2$  and  $80^\circ\text{C}$ ). These results demonstrate the versatility and potential application of these bimetallic tandem hydroformylation/acetalization catalytic systems for the direct transformation of a broad range of olefins into high-value products.

It should be noted that use of ethanol, which may be obtained from renewable sources, both as solvent and acetalization reagent, has the potential to increase the sustainability of the process.

### 2.3. Sequential Heterogeneous Hydroformylation/Acetalization of Olefins

Aiming to enhance the sustainability of the process, these studies pursued with the evaluation of the immobilized Rh and Fe catalysts onto iron magnetic nanoparticles (**CAT5** and **CAT 6**).

Table 2. Hydroformylation/acetalization of olefins.

Entry.	Olefin	Reaction Yield (%) <sup>[a]</sup>	
		Major Product (Isolated Yield)	Minor Products
1 <sup>[b]</sup>		 79 (70) (5a)	Oct-1-ene isomers: 4 Aldehydes: 11 Branched acetal: 6
2 <sup>[c]</sup>		 80 (74) (9a)	Aldehydes: 20
3 <sup>[c]</sup>		 57 (40) (10a)	Difunctionalized acetal (isomers): 33

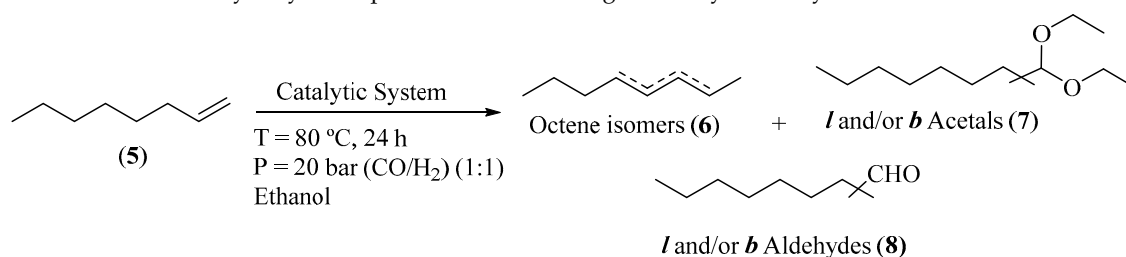
<sup>[a]</sup> Obtained by GC-MS analysis, conversions were  $\geq 99\%$  for all substrates. <sup>[b]</sup> Reaction conditions: olefin 3.00 mmol, CAT2 0.02 mmol, CAT1 0.05 mmol, alcohol 6 mL, 80 °C, 20 bar CO/H<sub>2</sub> (1:1) for 24 h, <sup>[c]</sup> Reaction conditions: olefin 1.50 mmol, CAT4 0.01 mmol, CAT1 0.05 mmol, ethanol 5 mL, 80 °C, 20 bar CO/H<sub>2</sub> (1:1) for 24 h.

Therefore, before the sequential catalytic studies, under heterogeneous conditions, the catalytic activity of CAT5 in hydroformylation and CAT6 in acetalization reactions was evaluated separately. Individually, the heterogeneous catalysts CAT5 or CAT6 were loaded into a high-pressure autoclave and kept at 30 bar (CO/H<sub>2</sub>) pressure for 2 h, at 80 °C. Then, after oct-1-ene addition, (CAT 5 experiment) or nonanal addition (CAT 6 experiment), the reactor was again pressurized with 20 bar of CO/H<sub>2</sub> gas (1:1) and heated to 80 °C under stirring. After 24 h, an aliquot was taken from the reaction crude and diluted with ethanol. Then, it was analyzed by gas chromatography using isooctane as external standard. All manipulations were performed under inert atmosphere.

The immobilized MNP@SiO<sub>2</sub>-NH-Rh(I)/N-Xantphos CAT5 revealed to be very active and selective, reaching 99% conversion, aldehyde chemoselectivity of 96% and 98% regioselectivity for the linear aldehyde (Table 3, Entry 1). Next, we evaluated MNP@SiO<sub>2</sub>-NH-[FeBr<sub>2</sub>{allyl-HC(pz)<sub>3</sub>}]<sub>2</sub>, CAT6, in the acetalization of commercial nonanal, using ethanol, under hydroformylation conditions, and 1,1-diethoxynonane was obtained in 90% yield (Table 3, Entry 2). Then, the combination of CAT5 and CAT6 was tested, by mixing them in an autoclave and using the general procedure described above. Under these experimental conditions, we obtained 92% of conversion, 54% of oct-1-ene isomers, and just 38% of aldehydes. Thus, the simultaneous use of CAT5 and CAT6 led to a significant loss of chemoselectivity concomitantly with no transformation into the desired acetal (Table 3, Entry 3). Contrarily, when CAT5 is used in the hydroformylation step and then removed with the aid of an external magnet from the reaction medium, (crude contains 96% of aldehydes; Table 3 Entry 1), the addition of CAT6 leads to the formation of acetals in 87% yield (Table 3, Entry 4). The lack of orthogonality observed exclusively under these heterogeneous conditions may be attributed to the presence of free residual NH<sub>2</sub> groups on the CAT6 magnetic nanoparticles surfaces that may coordinate with the Rh salt and thus affect the process selectivity. These results indicate that both CAT5 and CAT6 are

active and selective for the hydroformylation/acetalization process, when the reactions are performed in two sequential independent steps, Figure 6.

**Table 3.** Catalytic system optimization for heterogeneous hydroformylation/acetalization <sup>[a]</sup>.



Entry	Substrate	Catalyst	Conversion (%) <sup>[b]</sup>	Selectivity (%) <sup>[b]</sup> (I:b)		
				6	7	8
1 <sup>[c]</sup>	Oct-1-ene	CAT5	99	3	-	96(98:2)
2 <sup>[d]</sup>	Nonanal	CAT6	90	-	90(100:0)	10
3 <sup>[c],[d]</sup>	Oct-1-ene	CAT5 CAT6	92	54	-	38(75:25)
4 <sup>[e]</sup>	Nonanal	CAT6	90	2	87(99:1)	10(98:2)

<sup>[a]</sup> Reaction conditions: substrate (3.00 mmol), ethanol (6 mL), 80 °C, 20 bar CO/H<sub>2</sub> (1:1) for 24 h. <sup>[b]</sup> Obtained by GC-MS analysis using isooctane as an external standard. <sup>[c]</sup> CAT5 180 mg (≈0.02 mmol (Rh)) <sup>[d]</sup> CAT6 300 mg (≈0.04 mmol (Fe)) <sup>[e]</sup> In absence of *syn* gas (CO/H<sub>2</sub>) and using the reaction crude from entry 1, as substrate source, after catalyst CAT5 removal.

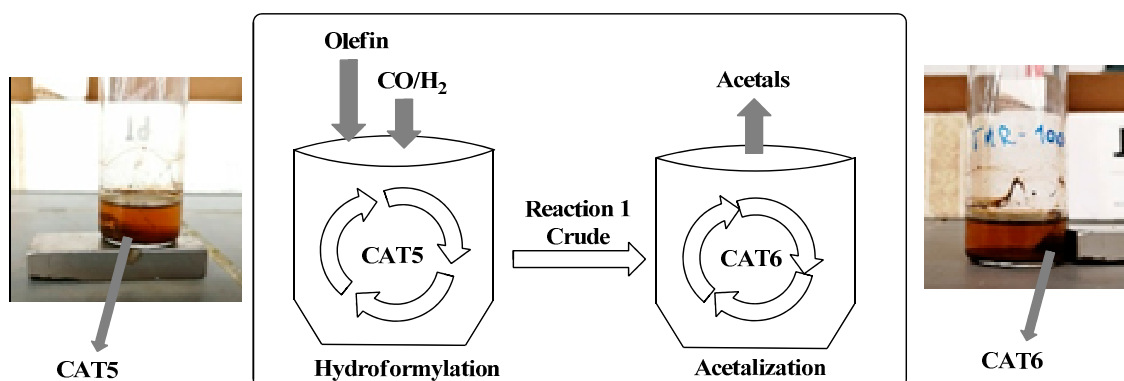


**Figure 6.** Two-step sequential system for hydroformylation/acetalization of olefins with reutilization of the catalysts through magnetic separation.

#### 2.4. Reutilization of Heterogeneous Catalysts

Pursuing our general goal for developing a sustainable system for the synthesis of acetals, we continue these studies with optimization of catalyst reutilization. After each cycle and under inert atmosphere, CAT5 was magnetically separated from hydroformylation reaction crude, which was then transferred to a vessel containing CAT6, for sequential acetalization. Both catalysts were reused in six consecutive cycles. Negligible loss of activity and selectivity was obtained, while in the acetalization step, a slight decrease was observed (Figure 7), which may be attributed to a small Fe leaching (1.6% determined by ICP) and/or loss during catalyst recovering process.

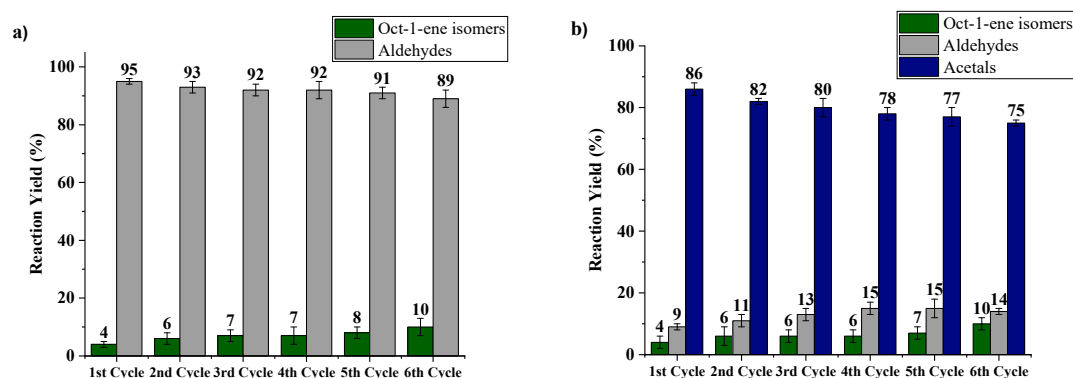


**Figure 7.** Two-step hydroformylation/acetalization of oct-1-ene, reutilization test: (a) hydroformylation step: 3 mmol oct-1-ene, CAT5 180 mg ( $\approx 0.02$  mmol [Rh]), 6 mL ethanol at 80 °C, 20 bar (CO:H<sub>2</sub>) for 24 h and (b) acetalization step: using hydroformylation step reaction crude, CAT6 300 mg ( $\approx 0.04$  mmol (Fe)) at 80 °C for 20 h.

### 3. Experimental

#### 3.1. Chemicals and Materials

All chemicals and materials were purchased from Sigma-Aldrich (Lisbon, Portugal), Fluorochem (Derbyshire, UK), or Strem Chemicals (Bischheim, France) and used as received. All solvents were dried and purified by standard methods. Ligands L1 (Xantphos) and L2 (triphenylphosphine) were purchased and used as received, while noncommercially available ligand L3 (*tris*[(R)-2'-(benzyloxy)-1,1'-binaphthyl-2-yl] phosphite) [49], tris(1-pyrazoyl)methane (1) [47], and tris(1-pyrazoyl) derivative 11 [53] were prepared according to the literature. All data are in agreement with corresponding literature. Catalysts CAT2, CAT3, and CAT4 were prepared in situ, using the known P-ligands and corresponding rhodium salts. Briefly, catalysts CAT2, CAT3, and CAT4 were prepared by mixing, in an autoclave, P-ligands (Figure 1, L1 = Xantphos, L2 = triphenylphosphine, or L3 = *tris*[(R)-2'-(benzyloxy)-1,1'-binaphthyl-2-yl] phosphite) with the commercially available pre-catalyst [Rh(acac)(CO)<sub>2</sub>], at 80 °C and 30 bar H<sub>2</sub>/CO (1:1), for 2 h, using ethanol as solvent, prior to the catalytic experiments.

#### 3.2. Instrumentation

Transmission electron microscopy (TEM) analyses were performed on a JEM 2100 apparatus (Jeol, Tokyo, Japan), at 200 kV, and size distributions of the materials were calculated by a statistical size distribution by manual analysis of enlarged images using the Imagetool software (Developed by Bruce McArthur, Digital Liquid Multimedia, Version 3.0) program (in triplicate). Thermogravimetric analysis was performed using a TG-DSC Perkin-Elmer STA6000 (Setaram, Caluire, France), with a heating rate of 10 °C min<sup>-1</sup> to a maximum temperature of 900 °C and 20 mL min<sup>-1</sup> nitrogen flux. The infrared spectra were performed in a Pike Miracle spectrometer (Pike Technologies, Madison, WI, USA) and each spectrum was obtained with a resolution of 4 cm<sup>-1</sup> (64 scans). Conversions and yields of hydroformylation and/or acetalization reactions were determined using an Agilent 7820 Gas Chromatograph system (Agilent, Santa Clara, CA, USA) equipped with a HP5 MS column (30 m × 0.25 mm × 0.25 μm) coupled to an Agilent 5975 MSD System Technologies (70 eV, Agilent, Santa Clara, CA, USA) using isooctane as an external standard. The inductively coupled plasma optical emission spectrometry (ICP-OES) analysis were conducted on an ICP-OES iCAP™ 7000 Series (ThermoFisher Scientific, Waltham, MA, USA).

#### 3.3. Synthesis of New Catalysts

##### 3.3.1. CAT1 Synthesis

**FeBr<sub>2</sub> and HC(pz)<sub>3</sub> (1) complexation:** To an ethanolic (10 mL) solution of FeBr<sub>2</sub> (251 mg, 1.63 mmol), an equimolar amount of HC(pz)<sub>3</sub> (360 mg, 1.68 mmol) in ethanol (10 mL) was slowly added under inert atmosphere of argon, the formation of a violet

precipitate is instantaneous. After stirring for 2 h, the solid was separated by filtration under inert atmosphere and dried under vacuum. The previously obtained powder was recrystallized in ethanol through solvent evaporation and crystals were obtained. Finally, the purple crystals were washed with cold ethanol and dried under vacuum (637 mg, 91%).  $^1\text{H-NMR}$  (400 MHz,  $\text{D}_2\text{O}$ )  $\delta$ (ppm): 9.22 (s, 1H), 8.56 (s, 3H), 7.83 (s, 3H), 7.09 (s, 3H).  $^{13}\text{C-NMR}$  (100 MHz,  $\text{D}_2\text{O}$ )  $\delta$ (ppm): 159.8, 143.1, 114.6, 74.2. HRMS (ESI):  $m/z$  = calcd. for  $\text{C}_{10}\text{H}_{10}\text{BrFeN}_6^+$  [M-Br] $^+$ : 348,9494; found: 348,9489 (Figures S1–S4).

### 3.3.2. Magnetic Nanoparticles Synthesis and Functionalization

Magnetite nanoparticles (MNP) were prepared, following a previously reported method [50]. Briefly, in a round-bottom flask, aqueous solutions of the iron precursors  $\text{FeCl}_3$  (aqueous) (10 mL, 1 mol/L) and  $\text{FeCl}_2$  (2.5 mL, 2 mol/L, acidic solution) were mixed with an aqueous solution of  $\text{NH}_4\text{OH}$  (250 mL, 1 mol/L) under mechanical stirring (10,000 rpm). All solutions were freshly prepared with deoxygenated water before use. After 30 min, under stirring, at room temperature, the MNP were magnetically recovered and washed with distilled water ( $3 \times 250$  mL), and redispersed in distilled water (250 mL). Oleic acid (2 mL, 7 mmol) in acetone (5 mL) was added dropwise to the reaction mixture under vigorous stirring for 30 min. The oleic acid-coated MNP were magnetically recovered and washed with acetone ( $3 \times 25$  mL) and dispersed in cyclohexane (15 mL). Then, the final solution was centrifuged for 30 min (at 2000 rpm) to remove any precipitate. Finally, a stock solution containing 72 mg of MNP/mL of cyclohexane was obtained, and a sample of this dispersion was then analyzed by transmission electron microscopy (Figure S5).

**Magnetite silica coating:**  $\text{MNP@SiO}_2$  were prepared by the reverse microemulsion method [51], and Igepal CO-520 (178.4 g), MNP (800 mg; 11.1 mL of stock solution in cyclohexane), and ammonium hydroxide (29%; 38 mL) were dispersed in cyclohexane (2.8 L) using ultrasounds. Then, tetraethyl orthosilicate (TEOS; 30.8 mL) was slowly added dropwise and the reaction occurred under slow stirring (300 rpm), for 16 hours. The resulting material was precipitated using methanol ( $\approx 250$  mL), recovered by centrifugation (7000 rpm, 30 min), and washed with ethanol. Finally, the  $\text{MNP@SiO}_2$  were dried for 24 h, at room temperature, and calcined at 500 °C for 2 hours.  $\text{MNP@SiO}_2$  were obtained (5.40 g) and analyzed by transmission electron microscopy (Figure S6).

**3-Chloropropyl-functionalization of  $\text{MNP@SiO}_2$ :** In a round-bottom flask,  $\text{MNP@SiO}_2$  (1.0 g) and (3-chloropropyl)triethoxysilane (CPTES) (0.5 mL; 2.07 mmol) were added in dry toluene (40 mL) and kept for 12 h, at 110 °C, under stirring.  $\text{MNP@SiO}_2\text{-Cl}$  were washed with ethyl acetate and acetonitrile followed by a drying process under vacuum for 24 h.  $\text{MNP@SiO}_2\text{-Cl}$  were characterized by thermal analysis (TG) and infrared spectroscopy (FTIR).

**3-Aminopropyl-functionalization of  $\text{MNP@SiO}_2$ :**  $\text{MNP@SiO}_2$  (1.0 g), 3-aminopropyltriethoxysilane (APTES; 0.5 mL; 2.13 mmol) and dry toluene (50 mL) were introduced in a round-bottom flask at reflux temperature for 12 h. Then,  $\text{MNP@SiO}_2\text{-NH}_2$  were washed with toluene and separated by centrifugation, the resulting material was finally dried at 100 °C for 20 h and characterized by thermal analysis (TG) and infrared spectroscopy (FTIR) (Figure S7).

### 3.3.3. CAT5 Synthesis

*N*-Xantphos (**2**) (435 mg, 0.79 mmol) was dissolved with dry DME (80 mL) in a Schlenk tube under inert atmosphere, then, dry sodium hydride (77 mg, 3.2 mmol) was slowly added to the solution and kept for 2 h at 80 °C under inert atmosphere. After that period,  $\text{MNP@SiO}_2\text{-Cl}$  (900 mg, 0.6 mmol of Cl groups) was added and the mixture was kept stirring for 12 h under inert atmosphere. After washing with DME ( $3 \times 50$  mL) and recovery with magnetic separation under inert atmosphere,  $[\text{Rh}(\text{acac})(\text{CO})_2]$  (180 mg, 0.7 mmol) and DME (50 mL) was added, and the mixture was kept under inert atmosphere for additional 6 h. The resulting material was again washed ( $5 \times 50$  mL) under inert atmosphere and dried under vacuum.

### 3.3.4. CAT6 Synthesis

**Complexation of 3 with FeBr<sub>2</sub> (complex 4):** To a 10 mL ethanolic solution of [FeBr<sub>2</sub>] (1.0 g, 3.5 mmol), an equimolar molar amount of tris-2,2,2-(1-pyrazoyl)ethoxyallyl, **3**, (1.0 g, 3.5 mmol) in ethanol (10 mL) was slowly added under inert atmosphere of argon, the formation of precipitate was instantaneous. After stirring for 2 h, the solid was filtered under inert atmosphere and dried under vacuum. Finally, the obtained orange (1.65 g, 95%) powder, **4**, was washed with cold ethanol and dried under vacuum. HRMS (EI):  $m/z = \text{calcd. for } C_{14}H_{16}BrFeN_6O^+ [M-Br]^+$ : 418,9918; found: 418,9911. 3.325 (Figures S8 and S9).

**Immobilization of iron complex 4 onto MNP@SiO<sub>2</sub>-NH<sub>2</sub> (CAT6):** The synthesis of immobilized Iron (II)/C-allyl-scorpionate type catalyst onto MNP was performed via hydroaminomethylation reaction. First, Rh(acac)(CO)<sub>2</sub> (6 mg, 0.02 mmol) and Xantphos (23.0 mg, 0.04 mmol) were incubated in a high-pressure reactor in anisole (5 mL), with 30 bar (CO/H<sub>2</sub>, 1:1), at 80 °C for 1 h. Then, complex **4** (1.0 g, 2.0 mmol), and the aminated nanoparticle, MNP@SiO<sub>2</sub>-NH<sub>2</sub> (900 mg, 1.3 mmol of amine groups) were added to the reactor under inert atmosphere. After addition of freshly dried toluene (10 mL) via cannula, the reactor was pressurized with 30 bar (CO/H<sub>2</sub>, 1:1) at constant pressure and kept at 65 °C for 48 h with vigorous magnetic stirring. After this period, the reactor was cooled to room temperature, degassed, and finally charged with H<sub>2</sub> (P = 30 bar) at 65 °C for additional 4 h. The reactor was then cooled to room temperature, depressurized, and opened in a glovebox under inert atmosphere. The **CAT6** material was isolated from the reaction medium by application of an external magnetic field. After removal of the supernatant, the remaining solid was washed with DME, anisole, and acetonitrile (3 × 20 mL) and dried under vacuum at room temperature for 24 h; the solid was then analyzed by TG-DSC and ICP-OES.

## 3.4. General Methods for the Hydroformylation/Acetalization of Alkenes

### 3.4.1. Homogeneous Bimetallic System

A 20 mL stainless steel autoclave was charged with [Rh(acac)(CO)<sub>2</sub>] (5.16 mg, 0.02 mmol), Xantphos (28.9 mg, 0.05 mmol) (**CAT2**), and [FeBr<sub>2</sub>{HC(pz)<sub>3</sub>}] (**CAT1**) (22.0 mg, 0.05 mmol). The autoclave was closed, and the air was removed using a vacuum pump. Ethanol (3 mL) was added via cannula and the autoclave was charged with 30 bar (CO:H<sub>2</sub>) and kept for 2 h at 80 °C. Then, the alkene (3 mmol) and 3 mL of dry ethanol were added through a cannula. After flushing the autoclave with CO/H<sub>2</sub>, it was pressurized with 20 bar of the same equimolar mixture of CO/H<sub>2</sub> gas and heated to 80 °C with magnetic stirring. After 24 h, the autoclave was cooled with icy water and the pressure was released. The crude reaction mixture was diluted with ethanol and analyzed by gas chromatography using isooctane as an external standard.

### 3.4.2. Heterogeneous One-Pot Bimetallic System

The desired amount of **CAT5** (180 mg 0.02 mmol Rh) and **CAT6** (300 mg 0.04 mmol Fe) was loaded into a 20 mL high-pressure autoclave, dispersed in ethanol (4 mL) and kept at 30 bar (CO/H<sub>2</sub>) pressure for 2 h, at 80 °C. Then, after substrate addition (3 mmol) dissolved in 2 mL of ethanol, the reactor was flushed and pressurized with 20 bar of CO:H<sub>2</sub> gas (1:1) and heated to 80 °C, under stirring. After 24 h, both catalysts were separated by magnetic separation and stored under inert atmosphere. An aliquot was taken from the reaction crude and analyzed by gas chromatography using isooctane as external standard and a complex mixture of products was observed.

### 3.4.3. Heterogeneous Sequential Process

The desired amount of **CAT5** (180 mg 0.02 mmol Rh) was loaded into a 20 mL high-pressure autoclave, dispersed in ethanol (4 mL) and kept at 30 bar (CO/H<sub>2</sub>) pressure for 2 h, at 80 °C. Then, after substrate addition (3 mmol) and 2 mL of ethanol, the reactor was flushed and pressurized with 20 bar of CO:H<sub>2</sub> gas (1:1) and heated to 80 °C under stirring. After 24 h, the catalyst was isolated from the reaction crude through magnetic separation and stored under inert atmosphere. Then, the reaction was transferred to another reaction

vessel containing **CAT6** (300 mg 0.04 mmol Fe) and kept for additional 24 h at 80 °C, under inert atmosphere. An aliquot was taken from the reaction crude and analyzed by gas chromatography, using isooctane as external standard. **CAT6** was also magnetically separated and stored under inert atmosphere.

#### 3.4.4. Reutilization Process

The above-described process was repeated for further five runs. The results are shown in Figure 6. The ICP analysis of initial and final **CAT5** Rh contents showed 0.9% Rh leaching, while ICP analysis of Fe **CAT6** showed 1.6% Fe leaching, after 6 runs.

## 4. Conclusions

For the first time, Rh(I)/P-ligand and Fe(II)/C-scorpionate catalysts were combined, in homogenous conditions. While Rh(I)/Xantphos and (Rh(I)/phosphite) efficiently allowed the hydroformylation of terminal and bulky olefins (including limonene's internal and external olefin bonds), respectively, the Fe(II)/C-scorpionate catalyst efficiently catalyzed the one-pot subsequent transformation into the corresponding acetals. These catalysts were further immobilized onto functionalized magnetic nanoparticles, where we highlight the use of catalytic hydroaminomethylation reaction to promote the efficient immobilization of the new Fe(II)-allyl-C-scorpionate species onto the aminated magnetic nanoparticle. The sequential process, using the immobilized catalysts, maintains its high activity and selectivity. Moreover, the system sustainability is largely improved by the easy magnetic separation/reutilization of Rh/P and Fe/C-scorpionate immobilized catalysts, which individually keep their activity/selectivity for six consecutive cycles. In sum, this study opens the way for the preparation of multi-functionalized acetals directly from olefins using reusable Rh/P and Fe/C-scorpionate catalysts, under mild reaction conditions.

This work further points out the utility of hydroformylation as central reaction for immobilization of other allyl metal complexes via hydroformylation/reductive amination.

**Supplementary Materials:** The following are available online at <https://www.mdpi.com/article/10.3390/catal11050608/s1>, Figure S1: <sup>1</sup>H-NMR spectrum of **CAT1** in D<sub>2</sub>O; Figure S2: <sup>13</sup>C-NMR spectrum of **CAT1** in D<sub>2</sub>O; Figure S3: HRMS-ESI spectrum of **CAT1**; Figure S4: IR spectrum of **CAT1** (FAR region) were the 252.6 cm<sup>-1</sup> is attributed to Fe-Br; Figure S5: TEM image of MNP and their corresponding size distribution histogram (≈7 nm); Figure S6: TEM image of MNP@SiO<sub>2</sub> and their corresponding size distribution histogram (≈23 nm); Figure S7. Comparative infrared spectra of MNP@SiO<sub>2</sub>-NH<sub>2</sub> and MNP@SiO<sub>2</sub>; Figure S8: HRMS-ESI spectrum of compound **4**; Figure S9: IR spectrum of complex **4** (Far region); Figure S10: <sup>1</sup>H-NMR spectrum of compound **9a** in CDCl<sub>3</sub>; Figure S11: <sup>13</sup>C-NMR spectrum of compound **9a** in (CD<sub>3</sub>)<sub>2</sub>CO.

**Author Contributions:** Conceptualization, M.M.P., A.J.L.P., and L.M.D.R.S.M.; methodology, M.M.P., L.M.D.R.S.M., and F.M.S.R.; validation, M.M.P., L.M.R., and T.M.R.M.; formal analysis, M.M.P., L.M.D.R.S.M., and A.J.L.P.; investigation, F.M.S.R. and L.D.D.; writing—original draft preparation, F.M.S.R., L.D.D., and M.J.F.C.; writing—review and editing, M.M.P., L.M.D.R.S.M., M.J.F.C., and F.M.S.R.; supervision, M.M.P.; project administration, M.M.P.; funding acquisition, M.M.P., L.M.R., and A.J.L.P. All authors have read and agreed to the published version of the manuscript.

**Funding:** This research was funded by Fundação para a Ciência e a Tecnologia (FCT) to Coimbra Chemistry Centre (UIDB/00313/2020) and to Centro de Química Estrutural (UIDB/00100/2020 and PTDC/QEQ-ERQ/1648/2014 projects). Fundação de Amparo à Pesquisa do Estado de São Paulo (FAPESP—grant 2016/16738-7). We are also grateful to PTDC/QUI-OUT/27996/2017. F.R. acknowledges the financial support from FCT (PD/BD/114340/2016 CATSUS—Catalysis and Sustainability PhD Program) and L.D. thanks Fundação de Amparo à Pesquisa do Estado de São Paulo (FAPESP) for post-doctoral grant (2019/13569-8). L.R. acknowledges the financial support from CAPES, CNPq, and INCT-Catálise. Access to TAIL-UC facilities funder under “QREN-Mais Centro Project ICT\_2009\_02\_012\_1890” is gratefully acknowledged.

**Conflicts of Interest:** The authors declare no conflict of interest.

## References

- Galván, A.; Fañanás, F.J.; Rodríguez, F. Multicomponent and multicatalytic reactions—A synthetic strategy inspired by nature. *Eur. J. Inorg. Chem.* **2016**, *9*, 1306–1313. [[CrossRef](#)]
- Lohr, T.L.; Marks, T.J. Orthogonal tandem catalysis. *Nat. Chem.* **2015**, *7*, 477–482. [[CrossRef](#)] [[PubMed](#)]
- Plass, C.; Hinzmann, A.; Terhorst, M.; Brauer, W.; Oike, K.; Yavuzer, H.; Asano, Y.; Vorholt, A.J.; Betke, T.; Gröger, H. Approaching bulk chemical nitriles from alkenes: A hydrogen cyanide-free approach through a combination of hydroformylation and biocatalysis. *ACS Catal.* **2019**, *9*, 5198–5203. [[CrossRef](#)]
- Bondžić, B.P. Rh catalyzed multicomponent tandem and one-pot reactions under hydroformylation conditions. *J. Mol. Catal. A-Chem.* **2015**, *408*, 310–334. [[CrossRef](#)]
- Franke, R.; Selent, D.; Börner, A. Applied hydroformylation. *Chem. Rev.* **2012**, *112*, 5675–5732. [[CrossRef](#)]
- Kalck, P.; Urrutigoity, M. Tandem hydroaminomethylation reaction to synthesize amines from alkenes. *Chem. Rev.* **2018**, *118*, 3833–3861. [[CrossRef](#)] [[PubMed](#)]
- Claver, C. *Rhodium Catalysis in Topics in Organometallic Chemistry*; Springer: Berlin/Heidelberg, Germany, 2018.
- Kollár, L.; Pongrácz, P. Tandem hydroformylation/aldol condensation reactions: Synthesis of unsaturated ketones from olefins. *J. Organomet. Chem.* **2018**, *866*, 184–188. [[CrossRef](#)]
- Pongrácz, P.; Bartal, B.; Kollár, L.; Mika, L.T. Rhodium-catalyzed hydroformylation in  $\gamma$ -valerolactone as a biomass-derived solvent. *J. Organomet. Chem.* **2017**, *847*, 140–145. [[CrossRef](#)]
- Torres, G.M.; Frauenlob, R.; Franke, R.; Börner, A. Production of alcohols via hydroformylation. *Catal. Sci. Technol.* **2015**, *5*, 34–54. [[CrossRef](#)]
- Almeida, A.R.; Dias, R.D.; Monteiro, C.J.P.; Abreu, A.R.; Gois, P.M.P.; Bayon, J.C.; Pereira, M.M. Rhodium-catalysed tandem hydroformylation/arylation reaction with boronic acids. *Adv. Synth. Catal.* **2014**, *356*, 1223–1228. [[CrossRef](#)]
- Liu, H.; Liu, L.; Guo, W.-D.; Lu, Y.; Zhao, X.-L. Phosphine-ligated Ir(III)-complex as a bi-functional catalyst for one-pot tandem hydroformylation-acetalization. *J. Catal.* **2019**, *373*, 215–221. [[CrossRef](#)]
- Wang, P.; Wang, D.L.; Liu, H.; Zhao, X.-L.; Lu, Y.; Liu, Y. Production of alcohols from olefins via one-pot tandem hydroformylation-acetalization-hydrogenolysis over bifunctional catalyst merging RuIII-P complex and RuIII Lewis acid. *Organometallics* **2017**, *36*, 2404–2411. [[CrossRef](#)]
- Li, Y.Q.; Wang, P.; Liu, H.; Lu, Y.; Zhao, X.-L.; Liu, Y. Co-catalysis of a bi-functional ligand containing phosphine and Lewis acidic phosphonium for hydroformylation-acetalization of olefins. *Green Chem.* **2016**, *18*, 1798–1806. [[CrossRef](#)]
- Wang, P.; Liu, H.; Li, Y.-Q.; Zhao, X.-L.; Lu, Y.; Liu, Y. Phosphonium-based aminophosphines as bifunctional ligands for sequential catalysis of one-pot hydroformylation-acetalization of olefins. *Catal. Sci. Technol.* **2016**, *6*, 3854–3861. [[CrossRef](#)]
- Vieira, C.G.; da Silva, J.G.; Penna, C.A.A.; dos Santos, E.N.; Gusevskaya, E.V. Synthesis of fragrance compounds from renewable resources: The aqueous biphasic hydroformylation of acyclic terpenes. *Appl. Catal. A* **2010**, *380*, 125–132. [[CrossRef](#)]
- Freixa, Z.; Pereira, M.M.; Pais, A.A.C.C.; Bayón, J.C. Evidence of a rhodium catalytic species containing a bridging 1,2-diphosphine in styrene hydroformylation. *J. Chem. Soc. Dalton Trans.* **1999**, *18*, 3245–3251. [[CrossRef](#)]
- de Freitas, M.C.; Vieira, C.G.; dos Santos, E.N.; Gusevskaya, E.V. Synthesis of fragrance compounds from biorenewables: Tandem hydroformylation-acetalization of bicyclic monoterpenes. *ChemCatChem* **2013**, *5*, 1884–1890. [[CrossRef](#)]
- Vieira, C.G.; dos Santos, E.N.; Gusevskaya, E.V. Synthesis of fragrance compounds from acyclic monoterpenes: Rhodium catalyzed hydroformylation and tandem hydroformylation/acetalization of linalool and citronellene. *Appl. Catal. A* **2013**, *466*, 208–215. [[CrossRef](#)]
- Munnik, P.; de Jongh, P.E.; de Jong, P.K. Recent developments in the synthesis of supported catalysts. *Chem. Rev.* **2015**, *115*, 6687–6718. [[CrossRef](#)] [[PubMed](#)]
- Börner, A.; Franke, R. *Hydroformylation: Fundamentals, Processes and Applications in Organic Synthesis*; VCH: Weinheim, Germany, 2016.
- Rodrigues, F.M.S.; Carrilho, R.M.B.; Pereira, M.M. Reusable catalysts for hydroformylation based reactions. *Eur. J. Inorg. Chem.* **2021**. [[CrossRef](#)]
- Hanf, S.; Rupflin, L.A.; Gläser, R.; Schunk, S.A. Current state of the art of the solid Rh-based catalyzed hydroformylation of short-chain olefins. *Catalysts* **2020**, *10*, 510. [[CrossRef](#)]
- Li, C.; Wang, W.; Yan, L.; Ding, Y. A mini review on strategies for heterogenization of rhodium-based hydroformylation catalysts. *Front. Chem. Sci. Eng.* **2018**, *12*, 113–123. [[CrossRef](#)]
- Molnár, Á.; Papp, A. Catalyst recycling - A survey of recent progress and current status. *Coord. Chem. Rev.* **2017**, *349*, 1–65. [[CrossRef](#)]
- Neves, A.C.B.; Calvete, M.J.F.; Pinho e Melo, T.M.V.D.; Pereira, M.M. Immobilized catalysts for hydroformylation reactions: A versatile tool for aldehyde synthesis. *Eur. J. Org. Chem.* **2012**, *32*, 6309–6320. [[CrossRef](#)]
- Sandee, A.J.; Reek, J.N.H.; Kamer, P.C.J.; van Leeuwen, P.W.N.M. A silica-supported, switchable, and recyclable hydroformylation-hydrogenation catalyst. *J. Am. Chem. Soc.* **2001**, *123*, 8468–8476. [[CrossRef](#)]
- Ricken, S.; Osinski, P.W.; Eilbracht, P.; Haag, R. A new approach to dendritic supported NIXANTPHOS-based hydroformylation catalysts. *J. Mol. Catal. A Chem.* **2006**, *257*, 78–88. [[CrossRef](#)]

29. Joumaa, A.; Gayet, F.; Garcia-Suarez, E.J.; Himmelstrup, J.; Riisager, A.; Poli, R.; Manoury, E. Synthesis of Nixantphos core-functionalized amphiphilic nanoreactors and application to rhodium-catalyzed aqueous biphasic 1-octene hydroformylation. *Polymers* **2020**, *12*, 1107. [[CrossRef](#)]
30. Polshettiwar, V.; Luque, R.; Fihri, A.; Zhu, H.; Bouhrara, M.; Bassett, J.-M. Magnetically recoverable nanocatalysts. *Chem. Rev.* **2011**, *111*, 3036–3075. [[CrossRef](#)] [[PubMed](#)]
31. Shaikh, M.N.; Bououdina, M.; Jimoh, A.A.; Aziz, M.A.; Helal, A.; Hakeem, A.S.; Yamania, Z.H.; Kimc, T.-J. The rhodium complex of bis(diphenylphosphinomethyl) dopamine-coated magnetic nanoparticles as an efficient and reusable catalyst for hydroformylation of olefins. *N. J. Chem.* **2015**, *39*, 7293–7299. [[CrossRef](#)]
32. Wang, P.; Chen, X.; Wang, D.-L.; Li, Y.-Q.; Liu, Y. Efficient and recyclable Rh-catalytic system with involvement of phosphine-functionalized phosphonium-based ionic liquids for tandem hydroformylation–acetalization. *Green Energy Environ.* **2017**, *2*, 419–427. [[CrossRef](#)]
33. Jin, X.; Zhao, K.; Cui, F.; Kong, F.; Liu, Q. Highly effective tandem hydroformylation–acetalization of olefins using a long-life Brønsted acid–Rh bifunctional catalyst in ionic liquid–alcohol systems. *Green Chem.* **2013**, *15*, 3236–3242. [[CrossRef](#)]
34. Norinder, J.; Rodrigues, C.; Börner, A. Tandem hydroformylation–acetalization with a ruthenium catalyst immobilized in ionic liquids. *J. Mol. Catal. A Chem.* **2014**, *391*, 139–143. [[CrossRef](#)]
35. Gorbunov, D.N.; Nenashva, M.V.; Sinikova, N.A.; Kardasheva, Y.S.; Maksimov, A.L.; Karakhanov, E.A. Tandem Hydroformylation–acetalization using a water-soluble catalytic system: A promising procedure for preparing valuable oxygen-containing compounds from olefins and polyols. *Russ. J. Appl. Chem.* **2018**, *91*, 990–995. [[CrossRef](#)]
36. Gorbunov, D.N.; Egazaryants, S.V.; Kardasheva, Y.S.; Maksimov, A.L.; Karakhanov, E.A. Synthesis of cyclic acetals by hydroformylation of oct-1-ene in the presence of polyols. *Russ. Chem. Bull.* **2015**, *64*, 943–947. [[CrossRef](#)]
37. Martins, L.M.D.R.S. C-scorpionate complexes: Ever young catalytic tools. *Coord. Chem. Rev.* **2019**, *396*, 89–102. [[CrossRef](#)]
38. Martins, L.M.D.R.S.; Pombeiro, A.J.L. Water-soluble C-scorpionate complexes – catalytic and biological applications. *Eur. J. Inorg. Chem.* **2016**, *15–16*, 2236–2252. [[CrossRef](#)]
39. Muñoz-Molina, J.M.; Belderrain, T.R.; Pérez, P.J. Group 11 tris(pyrazolyl)methane complexes: Structural features and catalytic application. *Dalton Trans.* **2019**, *48*, 10772–10781. [[CrossRef](#)] [[PubMed](#)]
40. Rocha, B.G.M.; Mac Leod, T.C.O.; Guedes da Silva, M.F.C.; Luzyanin, K.V.; Martins, L.M.D.R.S.; Pombeiro, A.J.L. NiII, CuII and ZnII complexes with a sterically hindered scorpionate ligand (TpmsPh) and catalytic application in the diastereoselective nitroaldol (Henry) reaction. *Dalton Trans.* **2014**, *43*, 15192–15200. [[CrossRef](#)] [[PubMed](#)]
41. Matias, I.A.S.; Ribeiro, A.P.C.; Ferraria, A.M.; Botelho do Rego, A.M.; Martins, L.M.D.R.S. Catalytic Performance of a Magnetic Core-Shell Iron(II) C-Scorpionate under Unconventional Oxidation Conditions. *Nanomaterials* **2020**, *10*, 2111. [[CrossRef](#)]
42. Matias, I.A.S.; Ribeiro, A.P.C.; Martins, L.M.D.R.S. Selective Oxidation of Ethane to Acetic Acid Catalyzed by a C-Scorpionate Iron(II) Complex: A Homogeneous vs. Heterogeneous Comparison. *Molecules* **2020**, *25*, 5642. [[CrossRef](#)]
43. Ottaviana, D.; Van-Dúnemb, V.; Carvalho, A.P.; Martins, A.; Martins, L.M.D.R.S. Eco-friendly cyclohexane oxidation by a V-scorpionate complex immobilized at hierarchical MOR zeolite. *Catal. Today* **2020**, *348*, 37–44. [[CrossRef](#)]
44. Ribeiro, A.P.C.; Martins, L.M.D.R.S.; Carabineiro, S.A.C.; Buijnsters, J.G.; Figueiredo, J.L.; Pombeiro, A.J.L. Heterogenized C-Scorpionate Iron(II) Complex on Nanostructured Carbon Materials as Recyclable Catalysts for Microwave-Assisted Oxidation Reactions. *ChemCatChem* **2018**, *10*, 1821–1828. [[CrossRef](#)]
45. Ribeiro, A.P.C.; Martins, L.M.D.R.S.; Kuznetsov, M.L.; Pombeiro, A.J.L. Tuning Cyclohexane Oxidation: Combination of Microwave Irradiation and Ionic Liquid with the C-Scorpionate [FeCl<sub>2</sub>(Tpm)] Catalyst. *Organometallics* **2017**, *36*, 192–198. [[CrossRef](#)]
46. Rodrigues, F.M.S.; Calvete, M.J.F.; Monteiro, C.J.P.; Carabineiro, S.A.C.; Maria, T.M.R.; Figueiredo, J.L.; Pereira, M.M. Hydroaminomethylation reaction as powerful tool for preparation of rhodium/phosphine-functionalized nanomaterials. Catalytic evaluation in styrene hydroformylation. *Catal. Today* **2020**, *356*, 456–463.
47. Reger, D.L.; Gratan, T.C.; Brown, K.J.; Little, C.A.; Lamba, J.J.S.; Rheingold, A.L.; Sommer, R.D. Syntheses of tris(pyrazolyl)methane ligands and [[tris(pyrazolyl)methane]Mn(CO)<sub>3</sub>]SO<sub>3</sub>CF<sub>3</sub> complexes: Comparison of ligand donor properties. *J. Organomet. Chem.* **2000**, *607*, 120–128. [[CrossRef](#)]
48. Silva, T.F.S.; Alegria, E.C.B.A.; Martins, L.M.D.R.S.; Pombeiro, A.J.L. Half-Sandwich Scorpionate Vanadium, Iron and Copper Complexes: Synthesis and Application in the Catalytic Peroxidative Oxidation of Cyclohexane under Mild Conditions. *Adv. Synth. Catal.* **2008**, *350*, 706–716. [[CrossRef](#)]
49. Carrilho, R.M.B.; Abreu, A.R.; Petöcz, G.; Bayón, J.C.; Moreno, M.J.S.M.; Kollár, L.; Pereira, M.M. New Binaphthyl-based C<sub>3</sub>-symmetric Chiral Hemilabile Monophosphite Ligands: Synthesis and Characterization of Their Platinum Complexes. *Chem. Lett.* **2009**, *38*, 844–845. [[CrossRef](#)]
50. Rossi, L.M.; Vono, L.L.R.; Silva, F.P.; Kiyohara, P.K.; Duarte, E.L.; Matos, J.R. A magnetically recoverable scavenger for palladium based on thiol-modified magnetite nanoparticles. *Appl. Catal. A* **2007**, *330*, 139–144. [[CrossRef](#)]
51. Jacinto, M.J.; Kiyohara, P.K.; Masunaga, S.H.; Jardim, R.F.; Rossi, L.M. Recoverable rhodium nanoparticles: Synthesis, characterization and catalytic performance in hydrogenation reactions. *Appl. Catal. A* **2008**, *338*, 52–57. [[CrossRef](#)]
52. Dias, L.D.; Carrilho, R.M.B.; Henriques, C.A.; Calvete, M.J.F.; Masdeu-Bulto-Claver, A.M.C.; Rossi, L.M.; Pereira, M.M. Hybrid metalloporphyrin magnetic nanoparticles as catalysts for sequential transformation of alkenes and CO<sub>2</sub> into cyclic carbonates. *ChemCatChem* **2018**, *10*, 2792–2803. [[CrossRef](#)]

53. Skalická, V.; Rybáčková, M.; Skalický, M.; Kvičalová, M.; Cvačka, J.; Březinová, A.; Čejka, J.; Kvičala, J. Polyfluoroalkylated tripyrazolylmethane ligands: Synthesis and complexes. *J. Fluor. Chem.* **2011**, *132*, 434–440. [[CrossRef](#)]
54. Pace, V.; Hoyos, P.; Castoldi, L.; de Maria, P.D.; Alcántara, A.R. 2-Methyltetrahydrofuran (2-MeTHF): A biomass-derived solvent with broad application in organic chemistry. *ChemSusChem* **2012**, *5*, 1369–1379. [[CrossRef](#)]
55. van Leeuwen, P.W.N.M.; Kamer, P.C.J. Featuring Xantphos. *Catal. Sci. Technol.* **2018**, *8*, 26–113. [[CrossRef](#)]
56. Kranenburg, M.; van der Burgt, Y.E.M.; Kamer, P.C.J.; van Leeuwen, P.W.N.M. New diphosphine ligands based on heterocyclic aromatics inducing very high regioselectivity in rhodium-catalyzed hydroformylation: Effect of the bite angle. *Organometallics* **1995**, *14*, 3081–3089. [[CrossRef](#)]
57. van Rooy, A.; Orij, E.N.; Kamer, P.C.J.; van Leeuwen, P.W.N.M. Hydroformylation with a rhodium/bulky Phosphite modified catalyst. A comparison of the catalyst behavior for oct-1-ene, cyclohexene, and styrene. *Organometallics* **1995**, *14*, 34–43. [[CrossRef](#)]
58. van Rooy, A.; de Bruijn, J.N.H.; Roobeek, K.F.; Kamer, P.C.J.; Van Leeuwen, P.W.N.M. Rhodium catalysed hydroformylation of branched 1-alkenes; bulky phosphites vs triphenylphosphine as modifying ligand. *J. Organomet. Chem.* **1996**, *507*, 69–73. [[CrossRef](#)]
59. Rodrigues, F.M.S.; Kucmierczyk, P.K.; Pineiro, M.; Jackstell, R.; Franke, R.; Pereira, M.M.; Beller, M. Dual Rh-Ru catalysts for reductive hydroformylation of olefins to alcohols. *ChemSusChem* **2018**, *11*, 2310–2314. [[CrossRef](#)] [[PubMed](#)]
60. Costa, G.N.; Carrilho, R.M.B.; Dias, L.D.; Viana, J.C.; Aquino, G.L.B.; Pineiro, M.; Pereira, M.M. Highly efficient Rh(I)/tris-binaphthyl monophosphite catalysts for hydroformylation of sterically hindered alkyl olefins. *J. Mol. Catal. A* **2016**, *416*, 73–80. [[CrossRef](#)]
61. Kamer, P.C.; Van Leeuwen, J.P.W.N.M.; Reek, J.N.H. Wide bite angle diphosphines: Xantphos ligands in transition metal complexes and catalysis. *Acc. Chem. Res.* **2001**, *34*, 895–904. [[CrossRef](#)] [[PubMed](#)]
62. Heck, R.F. Mechanism of arylation and carbomethoxylation of olefins with organopalladium compounds. *Acc. Chem. Res.* **1969**, *2*, 10–16. [[CrossRef](#)]
63. van der Veen, L.A.; Boele, M.D.K.; Bregman, F.R.; Kamer, P.C.J.; van Leeuwen, P.W.; Goubitz, K.; Fraanje, J.; Schenck, H.; Bo, C. Electronic effect on rhodium diphosphine catalyzed hydroformylation: The bite angle effect reconsidered. *J. Am. Chem. Soc.* **1998**, *120*, 11616–11626. [[CrossRef](#)]
64. Carrilho, R.M.B.; Neves, A.C.B.; Lourenço, M.A.O.; Abreu, A.R.; Rosado, M.T.S.; Abreu, P.E.; Eusébio, M.E.S.; Kollar, L.; Bayón, J.C.; Pereira, M.M. Rhodium/tris-binaphthyl chiral monophosphite complexes: Efficient catalysts for the hydroformylation of disubstituted aryl olefins. *J. Organomet. Chem.* **2012**, *698*, 28–34. [[CrossRef](#)]
65. Almeida, A.R.; Carrilho, R.M.B.; Peixoto, A.F.; Abreu, A.R.; Silva, A.; Pereira, M.M. Sequential reactions from catalytic hydroformylation toward the synthesis of amino compounds. *Tetrahedron* **2017**, *73*, 2389–2395. [[CrossRef](#)]